ACS APPLIED MATERIALS & INTERFACES

Research Article

www.acsami.org

Atomic Layer Deposited Lithium Silicates as Solid-State Electrolytes for All-Solid-State Batteries

Biqiong Wang,[†,‡] Jian Liu,[§] Mohammad Norouzi Banis,[†] Qian Sun,[†] Yang Zhao,[†] Ruying Li,[†] Tsun-Kong Sham,[*,‡] and Xueliang Sun[*,†]

[†]Department of Mechanical and Materials Engineering, University of Western Ontario, London, Ontario N6A 5B9, Canada

[‡]Department of Chemistry, University of Western Ontario, London, Ontario N6A 5B7, Canada

[§]Faculty of Applied Science, School of Engineering, University of British Columbia, Okanagan Campus, Kelowna, British Columbia V1V 1V7, Canada

Supporting Information

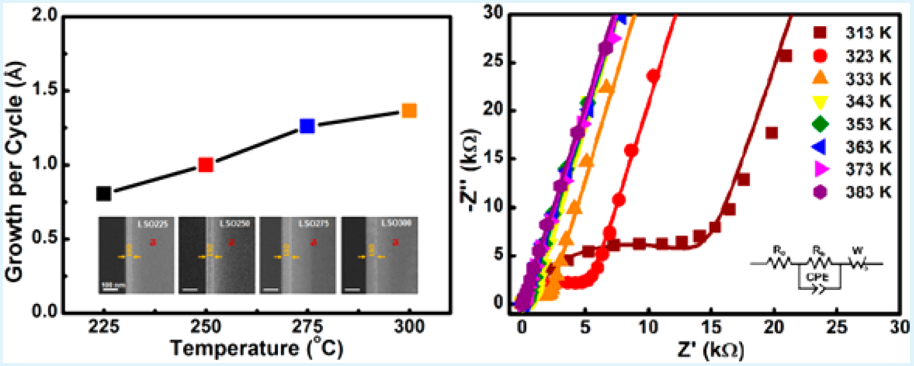

ABSTRACT: Development of solid-state electrolyte (SSE) thin films is a key toward the fabrication of all-solid-state batteries (ASSBs). However, it is challenging for conventional deposition techniques to deposit uniform and conformal SSE thin films in a well-controlled fashion. In this study, atomic layer deposition (ALD) was used to fabricate lithium silicate thin films as a potential SSE for ASSBs. Lithium silicates thin films were deposited by combining ALD Li_2O and SiO_2 subcycles using lithium *tert*-butoxide, tetraethylorthosilane, and H_2O as precursors. Uniform and self-limiting growth was achieved at temperatures between 225 and 300 °C. X-ray absorption spectroscopy analysis disclosed that the as-deposited lithium silicates were composed of SiO_4 tetrahedron structure and lithium oxide as the network modifier. X-ray photoelectron spectroscopy confirmed the chemical states of Li in the thin films were the same with that in standard lithium silicate. With one to one subcycle of Li_2O and SiO_2 the thin films had a composition close to Li_4SiO_4 whereas one more subcycle of Li_2O delivered a higher lithium content. The lithium silicate thin film prepared at 250 °C exhibited an ionic conductivity of 1.45×10^{-6} S cm^{-1} at 373 K. The high ionic conductivity of lithium silicate was due to the higher lithium concentration and lower activation energy.

KEYWORDS: *solid-state electrolytes, atomic layer deposition, X-ray absorption spectroscopy, lithium ion batteries, lithium silicates*

INTRODUCTION

Lithium ion batteries (LIBs) have led the revolutionary development of portable electronics in the past two decades due to their high energy density. Tremendous attention has also been directed toward improving LIBs to meet the stringent demands of hybrid electric vehicles (HEV), electric vehicles (EV), and grid energy storage systems. Deliberate and incremental progress has been made in optimizing the existing technology and the discovery of novel advanced battery materials.[1,2] One significant part of the research is ASSBs, where conventional liquid electrolyte is replaced by SSE. Liquid electrolytes carry inherent safety issues like flammability and risks of leakage, which will be eliminated by utilizing SSEs. In addition, the ASSBs provide more flexibility in battery design in order to pursue higher energy density and longer cycle life.[3−5] SSEs have primarily been incorporated in planar thin film batteries.[6,7] But the areal energy density is limited by the two-dimensional design. The advent of 3D architecture enables increased energy storage in a small footprint area. Moreover, miniaturization of power sources can give rise to an enormous market expansion of microelectronics.[3,8] Despite a few 3D configurations proposed so far, it is still challenging to fabricate conformal electrodes and electrolytes in such design for 3D ASSBs.[9−12]

ALD has been widely used for depositing conformal pinhole-free thin films on high-aspect-ratio 3D structures. Vaporized

Received: May 19, 2017
Accepted: July 27, 2017
Published: July 27, 2017

DOI: 10.1021/acsami.7b07113
ACS Appl. Mater. Interfaces 2017, 9, 31786−31793

precursors are sublimed and introduced into the deposition chamber alternatively. Saturated surface reactions based on the vapor-phase deposition dictate self-limiting film growths, therefore offering precise thickness control down to angstrom and tunable stoichiometry. The saturated and self-limiting surface reactions also ensure excellent coverage and uniformity on 3D substrates.[13−15] So far, various ALD processes have been established to synthesize different active materials as battery components.[7,16−18] Foremost, SSE is an indispensable component in ASSBs. Great efforts have been devoted to preparing lithium-containing thin films as SSEs by ALD, which remains to be challenging due to the limited choices of precursors and their different temperature windows.[15] Putkonen et al. first reported successful synthesis of Li_2CO_3 by ALD after the evaluations of a few lithium organic compounds as lithium precursors, promoting the rapid progress of ALD in lithium-containing systems.[19] Later on, lithium lanthanum titanate was deposited by combining the subcycles of TiO_2 ($TiCl_4$−H_2O), La_2O_3 ($La(thd)_3$−O_3), and Li_2O (LiO^tBu−H_2O).[20] Other lithium-containing compounds, lithium phosphate, lithium silicate, and $LiNbO_3$,[21−27] have been deposited by applying the similar strategy of combining ALD processes to obtain multicomponent oxides. Besides, there have been significant progress in ALD synthesis of active electrode materials. As an example, we have reported that TiO_2/Li_3PO_4 nanocomposites by ALD presented outstanding electrochemical performance as anodes for LIBs.[28] Cathode materials including $LiFePO_4$, $LiCoO_2$, and lithium manganese oxides have also been developed via ALD.[7,16,29]

The ionic conductivity of SSEs must be evaluated before being used in all-solid-state lithium ion batteries. A protocol measurement of the ionic conductivity of thin films by ALD was first demonstrated by Aaltonen et al.[21] Li_2O−Al_2O_3 thin film presented an ionic conductivity at the order of 10^{-7} S cm^{-1} at 573 K after 5 h annealing at 700 °C.[21] The high temperature required in postannealing, however, can be detrimental to the thin films or the substrates (the electrodes) due to the occurrence of film cracking resulting from thermal stress. Henceforth, glassy SSEs have become promising candidates considering that the easy film formation does not require harsh post-heat treatment. Moreover, high ionic conductivity can be achieved for the as-prepared thin films. Several systems have been selected and studied.[30−32] In our previous work, we have successfully developed lithium tantalate and lithium phosphate thin films with an ionic conductivity of 2×10^{-8} and 3.3×10^{-8} S cm^{-1}, respectively, at room temperature (RT).[31,32] Recently, lithium phosphorus oxynitride (LiPON) SSE has been synthesized by plasma-enhanced ALD and thermal ALD. The ionic conductivity of LiPON was improved to the order of 10^{-7} S cm^{-1} at RT.[33−36]

Apart from the aforementioned glassy SSEs, lithium silicate glasses (Li_2O−SiO_2) possesses an "open" framework that allows isotropic lithium ion migration and thus promises good ionic conductivity. Ionic conductivity of lithium silicate ranges from 10^{-8} to 10^{-6} S cm^{-1} depending on the Li_2O and SiO_2 compositions.[37−40] Furthermore, lithium silicate is relatively stable in contact with lithium metal, thus avoiding possible reduction at negative electrode.[39,40] Hämäläinen et al. established a process for lithium silicate with a stoichiometry close to lithium metasilicate ($Li_{2.0}SiO_{2.9}$) using lithium hexamethyldisilazide [LiHMDS] as both lithium and silicon sources and ozone as the oxidant.[23] In this study, we achieved the lithium silicate (LSO) thin film growth with an alternative ALD recipe based on lithium *tert*-butoxide (LiO^tBu), with tetraethylorthosilane (TEOS) as Si source. Local electronic structure of the ALD lithium silicate thin films was studied by X-ray absorption near-edge structure (XANES). The ionic conductivity of the amorphous LSO deposited at different temperatures was evaluated.

EXPERIMENTAL SECTION

Lithium silicate thin films were deposited in a Savannah 100 ALD system (Cambridge Nanotech Inc.) with nitrogen as the carrier and purging gas. The ALD subcycles of Li_2O and SiO_2 were combined. The Li_2O subcycle consisted of lithium *tert*-butoxide [LiO^tBu, $(CH_3)_3COLi$] as lithium source and H_2O as oxidant while tetraethylorthosilane (TEOS) and water were precursors for the SiO_2 ALD subcycle. LiO^tBu and TEOS were sublimed at a source temperature of 170 and 65 °C, respectively. The manifold was kept at 190 °C. Four different deposition temperatures were carried out, i.e., 225, 250, 275, and 300 °C, while the pulse time of LiO^tBu, TEOS, and water remained at 1, 2, and 1 s, respectively. One subcycle of Li_2O and one subcycle of SiO_2 composed one full ALD cycle. 10 s of nitrogen purge was used subsequently after each precursor. Silicon (100) substrates were cleaned using a stepwise acetone, ethanol, and water rinse procedure and then blown dry by N_2. Powder-based carbon nanotubes (CNTs) as substrates were refluxed in nitric acid (HNO_3, 70%) for 3 h at 120 °C in order to remove the residual catalyst involved in the growth of CNTs. Then the treated CNTs were washed by deionized water, dispersed in ethanol, drop-casted on Al foil, and dried overnight in air.

The cross section of thin films on Si substrates was observed using a field-emission scanning electron microscope (Hitachi-4800). The average thickness was measured and calculated from six randomly selected spots of each film. A Bruker D8 Advance X-ray diffraction (XRD) with Cu Kα X-ray source was employed to examine the crystal structure of the thin films on Si. X-ray photoelectron spectroscopy (XPS) [Kratos Axis Ultra Al (alpha) spectrometer] was employed to obtain the stoichiometry of the lithium silicates on CNTs. All the XANES study in this work was conducted in Canadian Light Source (CLS) on the Soft X-ray Microcharacterization Beamline (SXRMB). A InSb (111) crystal monochromator was set up for measuring Si K-edge. Total electron yield (TEY) and X-ray fluorescence yield (FLY) spectra were collected. All XANES spectra were normalized to the incident photon flux.

For impedance testing, lithium silicates thin films were sandwiched between sputtered Au layers (~50 nm) on glass substrates. All the LSO thin films were deposited to be 130 ± 2 nm thick. The effective planar area of sandwiched SSE was 4 × 4 mm^2. Electrochemical impedance spectroscopy (EIS) was acquired by a CHI electrochemistry workstation. The testing frequency decreased from 200 kHz to 100 mHz within a temperature window of 303−373 K (10 K step).

RESULTS AND DISCUSSION

Lithium silicates thin films grown on silicon at 225 °C (LSO225), 250 °C (LSO250), 275 °C (LSO275), and 300 °C (LSO300) were examined by SEM. Figure 1a shows the film thickness plotted against the ALD cycle number, which exhibits a linear correlation after fitting the data. It is indicative of a self-saturated growth, and thus a successful ALD process has been achieved at all four temperatures.[13] The cross-section views of lithium silicates thin films after 500 ALD cycles on Si substrates are displayed in Figure 1c−f. Uniform depositions can be seen at all four temperatures. The thicknesses of LSO225, LSO250, LSO275, and LSO300 thin films are measured to be 39, 49, 62, and 68 nm, respectively. ALD processes of SiO_2 using TEOS and water at low temperatures have been reported only in the presence of the NH_3 catalyst.[41−43] The Si−OH* surface species are reported to have strong interactions with Lewis bases like ammonia, and therefore the SiO−H chemical bond is

DOI: 10.1021/acsami.7b07113
ACS Appl. Mater. Interfaces 2017, 9, 31786−31793

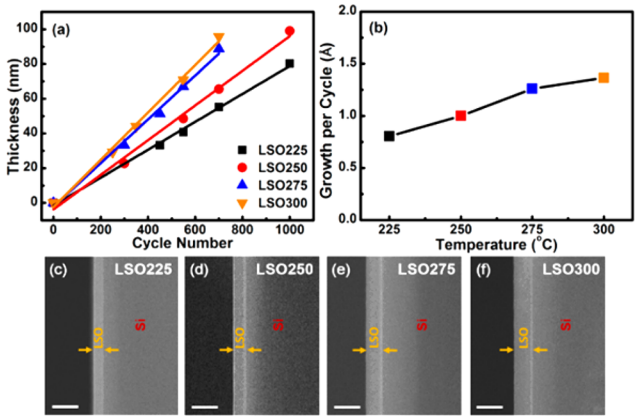

Figure 1. (a) Thickness of LSO thin films plotted against ALD cycle number; (b) growth per cycle of LSO at different deposition temperature; SEM pictures of the cross section of LSO thin films on silicon at (c) 225 °C (LSO225), (d) 250 °C (LSO250), (e) 275 °C (LSO275), and (f) 300 °C (LSO300) after 500 ALD cycles. The scale bar is 100 nm.

weakened, making the oxygen a stronger nucleophile.[13,41] Interestingly, no deposition was observed when the SiO_2 subcycle was conducted solely without the Li_2O subcycle. This might be ascribed to the similar mechanism. By introducing the Li_2O subcycle, a Lewis base environment might be created to facilitate the ligands removal during the TEOS subcycle.[26,30,42] The slope of the linear fitting lines represents the growth per cycle (GPC), as shown Figure 1b. A GPC of 0.80, 1.00, 1.26, and 1.36 Å is obtained for LSO225, LSO250, LSO275, and LSO300, respectively. A higher growth rate of lithium silicate is observed at a higher temperature. The reason could be that at elevated temperatures the ligand exchange reaction is promoted and the reactivity of LiO^tBu and TEOS is higher, leading to faster thin film growth.[13,23,31] When two subcycles of Li_2O were applied with one SiO_2 subcycle at 250 °C (denoted as LSO250-2), the GPC was increased to 2.57 Å (Figure S1a). The difference of GPC between LSO250 and LSO250-2 cannot be simply assigned to the extra one Li_2O subcycle considering its "catalyzing effect" on the growth of SiO_2 proposed above. This mechanism makes it difficult to isolate the study of the growth of SiO_2. Hence, we only focused on the effect of different ALD parameters on the electronic structures and the electrochemical performances of deposited thin films.

XANES at the Si K-edge was investigated the chemical environment of Si in the lithium silicate thin films. Si K-edge XANES involves the process that Si 1s electrons are excited into unoccupied states in the conduction band. The spectral features result from the dipole excitation of the core electrons to the bound and quasibound states and are related to the local structure and bonding environment of the absorbing atom. The chemical change could be determined by the shift of edge jump threshold or the position of the first resonance (known as the whiteline).[44−50] Spectra in Figures 2a and 2c were collected in total electron yield (TEY) mode while those in Figures 2b and 2d were in fluorescence yield (FLY) mode. TEY measures the total yield of photoelectrons, Auger electrons, and secondary electrons (dominant), revealing the information from several nanometers deep from the surface due to the shallow electron escape depth. On the other hand, FLY detects outgoing fluorescent X-rays which has 2 orders of magnitude increase in attenuation length in the solid than electrons, revealing bulk sensitive information.[47]

All the XANES spectra of the as-deposited thin films exhibited three main features, denoted as peak A, B, and C. First, comparing the four TEY spectra in Figure 2f, the whitelines of quartz SiO_2 and nano SiO_2 powders at 1846.8 eV agree well with the literature and can be attributed to the transition of Si 1s electrons to the antibonding 3p-like states (t_2) according to the dipole selection rules.[44−46] Below the

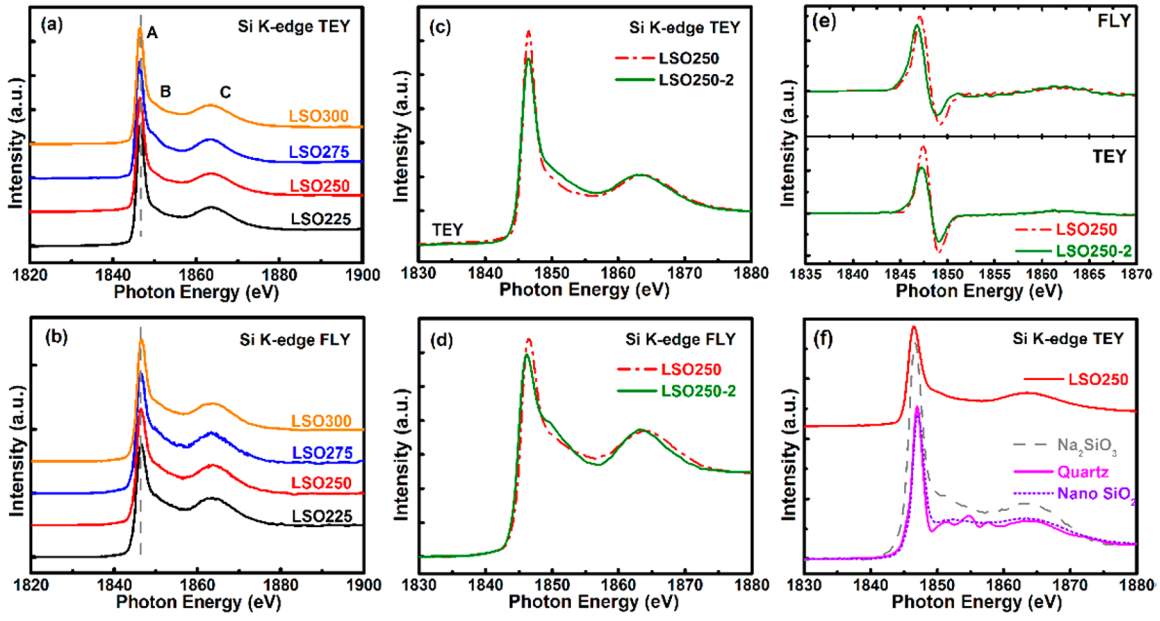

Figure 2. Si K-edge TEY XANES spectra at of lithium silicate thin films deposited (a) at different temperatures, (c) with different Li subcycle numbers, and (f) standard powders (Na_2SiO_3, quartz, and nano SiO_2). Si K-edge FLY XANES spectra at of lithium silicate thin films deposited (b) at different temperatures and (d) at 250 °C with different Li subcycle number. (e) First-derivative spectra plotted from TEY and FLY spectra of LSO250 and LSO250-2.

DOI: 10.1021/acsami.7b07113
ACS Appl. Mater. Interfaces 2017, 9, 31786−31793

edge, there is a weak shoulder peak arising from the forbidden transition from Si 1s to 3s-like states (a_1).[44,46] By introducing alkaline metals into the compound, the whiteline of LSO250 presented a red-shift of ~0.4 eV, consistent with the findings of Henderson et al.[45,48] A shift of the edge to lower energy in the spectra indicates a decrease in polymerization due to the addition of alkaline metal as a network modifier.[45,48] Besides, features in the spectrum of LSO250 resemble those for Na_2SiO_3 and standard lithium silicates in refs 45, 48, and 50, suggesting Si in the lithium silicate thin films exists in similar tetrahedral oxygen ligand environment.

Second, the TEY spectra in Figure 2a show the same resonances A, B, and C. Peak A locates at the same position of 1846.4 eV, which is identified to be the 1s to t_2 transition for the four-coordinated Si. No shift is observable, which implies the same local structure Si^{4+} bonded with four oxygens on the surface in the thin films deposited at different temperatures.[45,48] The only peak B (~1849.4 eV) between A and C instead of the well-resolved features seen in quartz is present. Essentially spin-forbidden transitions of Si 1s electrons to empty 3d states account for the features in this region, which is likely arising from local distortion. The alleviated distortion of the SiO_4 tetrahedron in amorphous systems and nano powders gives less chance for the overlapping of unoccupied 3p-like features with the 3d states, generating less symmetry-forbidden shape resonance. Therefore, the patterns are flattened out, indicating the amorphous nature of the thin film structures.[46,47] This was further verified by low-angle X-ray diffraction, where no diffraction patterns were found in the spectra, confirming the absence of long-range order.[28] Furthermore, the relative intensity of peak A to B remains almost the same for the four spectra. Based on Henderson and Li et al.'s work on the alkaline silicates, the network modifier in our case is only Li_2O in the binary glass. The ratio of peak A to B implies similar Li_2O content in the thin films prepared at different temperatures.[45,46,48] The FLY spectra in Figure 2b further substantiate the discussions above. The FLY XANES spectra suffer from the thickness effect, where the photon is self-absorbed by the thin films. The intensity of the whiteline is therefore reduced, and all the features are broadened.[47] Nevertheless, a comparison between TEY and FLY spectra disclose similar electronic structure of Si at the surface and in the bulk of the LSO samples.

XANES spectra of LSO250 and LSO250-2 are compared in Figure 2c–e. First, peaks A, B, and C experience a shift to lower energy in both TEY and FLY spectra when the ALD subcycle number of Li_2O increase from 1 to 2. The shift of ~0.3 eV is easily observable in the first-derivative spectra shown in Figure 2e. By increasing the Li_2O subcycle number, a higher Li to Si content ratio would be expected theoretically. The Li element is very electropositive, which will contribute more electrons toward Si. Si could exist in a chemical state a little lower than 4+ in the context of a Li-richer environment in LSO250-2, which can explain the red-shift of the whitelines as well as the edge jump. The shift also presages a possible lower degree of polymerization of SiO_4 tetrahedron, which is in good agreement with the effect of additional network modifier mentioned above.[45,46,48,50] The conclusion is further confirmed by the decrease of peak intensity of peak A to B from LSO250 to LSO250-2.[48,51,52] In addition, peak C is narrower and of higher intensity for LSO250-2 compared with LSO250. The higher lithium content might lead to an improvement in local order.[45,53]

To further analyze the chemical compositions of LSO, XPS was conducted using CNTs as substrates instead of Si wafers to avoid the interference of the background Si signal. XPS survey scans are provided in the Supporting Information. The peaks for C 1s and some oxygen signals are from the CNTs substrates and the functional groups attached. Apart from it, the thin films consist of the elements Li, Si, and O. The atomic ratio of Li to Si is calculated from the atomic percentage and lists 3.25, 3.74, 3.57, 3.51, and 5.84 corresponding to LSO225, LSO250, LSO275, LSO300, and LSO0250-2, respectively. The four lithium silicate thin films with one subcycle of Li_2O resemble a close stoichiometry to Li_4SiO_4 considering the XPS and the XANES results.[54−56] With two subcycles of Li_2O, a much higher lithium content is obtained, which coincides very well with the conclusions from the XANES spectra. Figure 3 shows

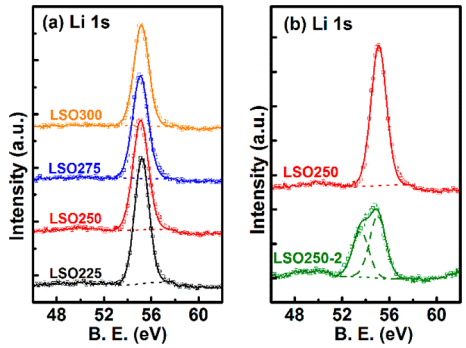

Figure 3. Deconvolution of Li 1s XPS spectra of lithium silicate thin films deposited (a) at different temperatures and (b) with different Li subcycle numbers.

the Li 1s high-resolution spectra with the deconvolution of the peaks. In Figure 3a, only one sharp and symmetric peak can be detected at 55.2 eV for all four spectra of thin films deposited at the four temperatures, indicating there is solely one chemical state (Li−O) in each sample. The single peak can be designated to that of lithium silicate (Li_4SiO_4) referring to the literature.[54−56] Also, no evident shift of the peak position can be seen among the four spectra which means the chemical state of Li in LSO is similar to that in standard Li_4SiO_4. Moreover, Figure 3b includes the Li 1s XPS spectra of LSO250 and LSO250-2. Differing from the spectrum of LSO250, the deconvolution shows that another peak emerges at a lower energy of 53.6 eV, except the one belonging to lithium silicate. The extra peak can be assigned to lithium oxide (Li_2O).[57−59] Therefore, the Li element in $Li_{5.84}SiO_z$ (LSO250-2) exists in two different environments, namely Li−O−Li (44%) and Li−O−Si (56%). The occurrence of Li−O−Li arised from the extra Li_2O subcycle in the ALD process. Both the quantitative and qualitative results of XPS are in excellent accordance with the XANES results.

Ionic conductivities of LSO thin films were measured by EIS. Figure 4a–e displays the Cole−Cole plots acquired at a temperature range from 313 to 383 K, followed by the Arrhenius plot of the ionic conductivity (Figure 4f). At the high frequency region, one semicircle was presented, attributed to the bulk resistance. At the low frequency region, an inclined tail can be ascribed to the polarization of the electrode−electrolyte interface. One important point to note is that this feature is typical of an ionic conductor when an open circuit diffusion takes place by using an ionic blocking electrode (Au for instance).[32,60] The impedance plots were fitted using an

DOI: 10.1021/acsami.7b07113
ACS Appl. Mater. Interfaces 2017, 9, 31786−31793

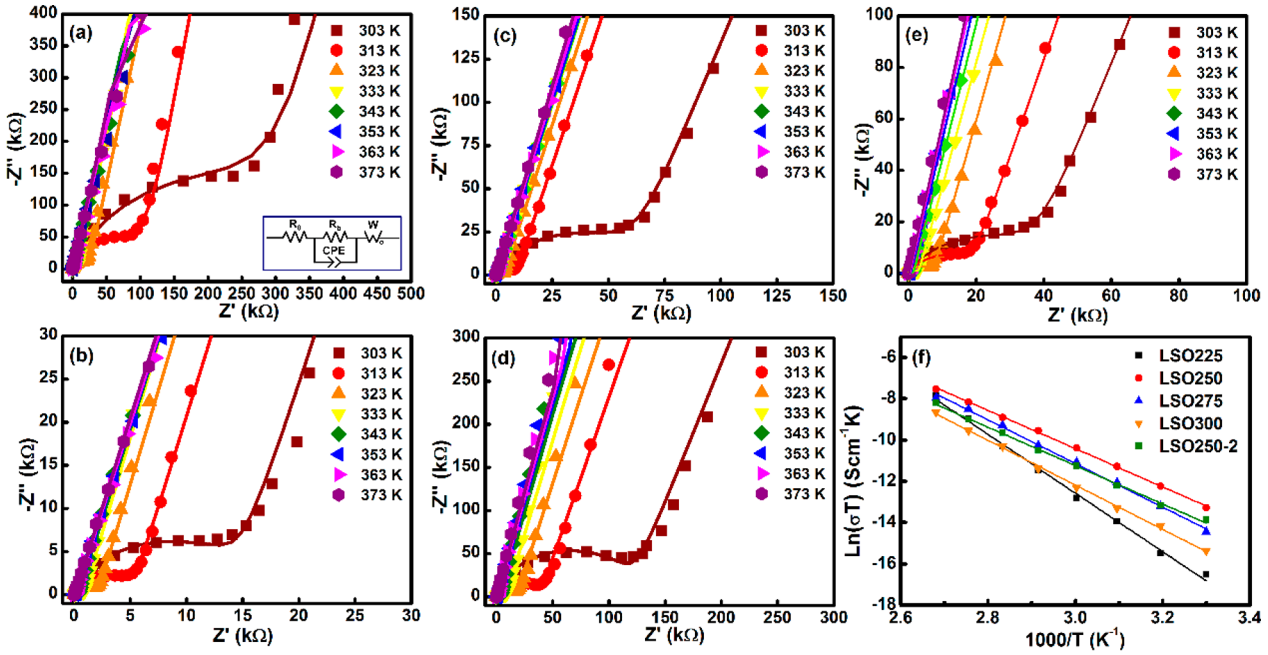

Figure 4. EIS plots of LSO thin films (a) LSO225, (b) LSO250, (c) LSO275, (d) LSO300, and (e) LSO250-2. (f) Arrhenius plots measured from 313 to 383 K (solid lines were simulated to fit the measured scattered points).

equivalent circuit depicted in the inset of Figure 4a, where R_0 and R_b denote the contact ohmic resistance and the bulk resistance of the electrolytes. A constant-phase element (CPE) was employed in the circuit, which represents the resultant bulk capacitance of the LSO thin films. W is the finite length Warburg element, occurring when charge carriers diffuse through the solid.[61]

The Li^+ conductivity of LSO thin films was calculated by applying the empirical R_b values into the equation $\sigma = d/(AR_b)$ wherein d = 130 nm and A = sandwiched area between the gold electrodes.[21,31,32] Comparing the thin films deposited with one Li subcycle, thin films LSO225, LSO250, LSO275, and LSO300 deliver an ionic conductivity of 1.05×10^{-6}, 1.45×10^{-6}, 9.41×10^{-7}, and 4.69×10^{-7} S cm^{-1}, respectively, at the maximum measuring temperature 373 K (100 °C), among which thin film LSO250 exhibits the highest value. Similarly, at the minimum measuring temperature 303 K (30 °C), the ionic conductivity measures to be 2.18×10^{-10}, 5.72×10^{-9}, 1.73×10^{-9}, and 7.06×10^{-10} S cm^{-1} for thin films LSO225, LSO250, LSO275, and LSO300, respectively. Although the ionic conductivities are of similar level, the best ionic conductivity can still be obtained from thin film LSO250. The reason can be associated with the lithium content of the as-prepared thin films. In silicate glass solid-state electrolyte systems, the elementary structural unit (SU) is SiO_4 tetrahedron sharing bridging oxygens (BO). A continuous 3D network over the entire volume forms. Introduction of alkali oxides leads to the disruption of the Si−O−Si bonds and consequently the formation of non-bridging oxygens (NBO), which would be beneficial to the conductivity. To improve the conductivity, one critical factor is the charge carrier concentration, which is lithium in this case. Among the four lithium silicate thin films, LSO250 has the highest lithium to silicon ratio (3.74), which is also the closest stoichiometry to Li_4SiO_4.[37,39,62−64] It is worth mentioning that to a certain degree a higher content of lithium might give rise to a better ionic conductivity, primarily owing to a reduced activation energy.[62,65−68] The value of E_a was calculated from the slope of the linear lines (Figure 4f), which are 1.22, 0.80, 0.91, and 0.93 eV for LSO225, LSO250, LSO275, and LSO300, respectively. The measured values are consistent with the range of E_a of lithium silicate glasses.[37,65−67,69] This provides further evidence for the above theory that LSO250 indeed has the lowest activation energy.

Furthermore, the ionic conductivity of LSO250-2 was also evaluated and is presented in Figure 4e, which varied from 3.13 $\times 10^{-9}$ to 7.46 $\times 10^{-7}$ S cm^{-1} from 303 to 373 K. The ionic conductivity of LSO250-2 is lower than that of LSO250, albeit LSO250-2 has a stoichiometry of $Li_{5.84}SiO_z$ which contains much more Li than LSO250. However, the activation energy of thin films LSO250-2 is 0.799 eV, almost the same with that of LSO250 (0.797 eV to be exact). The possible reasons are the following. First, ion motion in disordered solids can be described by activated hopping between charge-compensating sites. Conventionally, point defects form based on two models which are Schottky and Frankel processes. The former one involves cation−anion vacancy pairs while the latter relates to cation or anion vacancy−interstitial pairs. The amount of the defects affects the concentration of charge carries.[62,70] When there are much more equivalent sites than the available mobile ions to fill in, increasing the mobile ion density would benefit the ionic conductivity. The creation of NBO provides extra hopping sites and lowers the activation energy. However, to a certain degree, extra lithium into the system does not necessarily mean an increase in the mobile ion concentration, but probable occupants that "block" the possible diffusion pathways (vacancies). Meanwhile, the highest potential barrier that the ions have to conquer in diffusion could remain almost unchanged.[39,62,70] With the above being said, there is still severe paucity in the information on the mechanisms behind ion dynamics in amorphous ion conductors. Further studies and calculations are urged to advance the understanding of glassy solid-state electrolytes.

DOI: 10.1021/acsami.7b07113
ACS Appl. Mater. Interfaces 2017, 9, 31786−31793

CONCLUSIONS

ALD prepared lithium silicate SSEs were achieved at 225, 250, 275, and 300 °C with LiO^{t}Bu, TEOS, and H_2O as sources. Linear growth was obained with a GPC of 0.80, 1.00, 1.26, and 1.36 Å, respectively. At a deposition temperature of 250 °C, the GPC was also obtained with increased Li_2O subcycle number, which was 2.57 Å. The presence of Li_2O subcycle helps facilitate the growth of SiO_2. XANES analysis showed that Si in thin films share the same SiO_4 tetrahedral structure from the surface to the bulk and the thin films were amorphous. By introducing lithium oxide as the network modifier, the polymerization degree or long-range order was decreased. Extra lithium affected the bonding structures around Si. XPS results gave the ratio of Li to Si which was closed to the stoichiometry of Li_4SiO_4, except LSO250-2 with a much higher lithium content. XPS also confirmed that all the as-deposited lithium silicate thin films existed in similar chemical structure as that in standard Li_4SiO_4. Furthermore, the Li^+ conductivity of the thin film solid-state electrolytes was measured. LSO250 exhibited the best conductivity of 5.72×10^{-9} S cm^{-1} at 303 K. Incorporation of more Li improved the ionic conductivity but only to a certain degree. It is expected that the lithium silicate thin films developed by ALD can find potential applications in 3D all-solid-state batteries.

ASSOCIATED CONTENT

Supporting Information

The Supporting Information is available free of charge on the ACS Publications website at DOI: 10.1021/acsami.7b07113.

LSO250-2 film thickness as a function of ALD cycle number, SEM of cross section of LSO250-2 on Si, deposition of LSO250 on CNTs, and XPS survey scans of LSO thin films (PDF)

AUTHOR INFORMATION

Corresponding Authors

*E-mail tsham@uwo.ca; Tel +1 519 661 2111 ext 86341 (T-K.S.).

*E-mail xsun@eng.uwo.ca; Tel +1 519 661 2111 ext 87759 (X.S.).

ORCID

Yang Zhao: 0000-0002-4148-2603

Xueliang Sun: 0000-0003-2881-8237

Notes

The authors declare no competing financial interest.

ACKNOWLEDGMENTS

This work was funded by the Nature Sciences and Engineering Research Council of Canada (NSERC), the Canada Research Chair Program, the Canada Foundation for Innovation (CFI), the Ontario Research Fund, the Canada Light Source (CLS) at the University of Saskatchewan, and the University of Western Ontario. CLS was supported by CFI, NSERC, NRC, CHIR, and the University of Saskatchewan.

REFERENCES

(1) Goodenough, J. B.; Park, K.-S. The Li-Ion Rechargeable Battery: A Perspective. *J. Am. Chem. Soc.* **2013**, *135* (4), 1167−1176.

(2) Erickson, E. M.; Ghanty, C.; Aurbach, D. New Horizons for Conventional Lithium Ion Battery Technology. *J. Phys. Chem. Lett.* **2014**, *5* (19), 3313−3324.

(3) Oudenhoven, J. F. M.; Baggetto, L.; Notten, P. H. L. All-Solid-State Lithium-Ion Microbatteries: A Review of Various Three-Dimensional Concepts. *Adv. Energy Mater.* **2011**, *1* (1), 10−33.

(4) Ferrari, S.; Loveridge, M.; Beattie, S. D.; Jahn, M.; Dashwood, R. J.; Bhagat, R. Latest Advances in the Manufacturing of 3D Rechargeable Lithium Microbatteries. *J. Power Sources* **2015**, *286*, 25−46.

(5) Sun, C.; Liu, J.; Gong, Y.; Wilkinson, D. P.; Zhang, J. Recent Advances in All-Solid-State Rechargeable Lithium Batteries. *Nano Energy* **2017**, *33*, 363−386.

(6) Bates, J. B.; Dudney, N. J.; Neudecker, B.; Ueda, A.; Evans, C. D. Thin-Film Lithium and Lithium-Ion Batteries. *Solid State Ionics* **2000**, *135* (2000), 33−45.

(7) Donders, M. E.; Arnoldbik, W. M.; Knoops, H. C. M.; Kessels, W. M. M.; Notten, P. H. L. Atomic Layer Deposition of LiCoO2 Thin-Film Electrodes for All-Solid-State Li-Ion Micro-Batteries. *J. Electrochem. Soc.* **2013**, *160* (5), A3066−A3071.

(8) Roberts, M.; Johns, P.; Owen, J.; Brandell, D.; Edstrom, K.; El Enany, G.; Guery, C.; Golodnitsky, D.; Lacey, M.; Lecoeur, C.; Mazor, H.; Peled, E.; Perre, E.; Shaijumon, M. M.; Simon, P.; Taberna, P.-L. 3D Lithium Ion Batteries—from Fundamentals to Fabrication. *J. Mater. Chem.* **2011**, *21* (27), 9876−9890.

(9) Nam, Y. J.; Cho, S. J.; Oh, D. Y.; Lim, J. M.; Kim, S. Y.; Song, J. H.; Lee, Y. G.; Lee, S. Y.; Jung, Y. S. Bendable and Thin Sulfide Solid Electrolyte Film: A New Electrolyte Opportunity for Free-Standing and Stackable High-Energy All-Solid-State Lithium-Ion Batteries. *Nano Lett.* **2015**, *15* (5), 3317−3323.

(10) Yang, Y.; Peng, Z.; Wang, G.; Ruan, G.; Fan, X.; Li, L.; Fei, H.; et al. Three-Dimensional Thin Film for Lithium-Ion Batteries and. *ACS Nano* **2014**, *8* (7), 7279−7287.

(11) Zhang, Y.; Lai, J.; Gong, Y.; Hu, Y.; Liu, J.; Sun, C.; Wang, Z. L. A Safe High-Performance All-Solid-State Lithium-Vanadium Battery with a Freestanding V2O5 Nanowire Composite Paper Cathode. *ACS Appl. Mater. Interfaces* **2016**, *8* (50), 34309−34316.

(12) Talin, A. A.; Ruzmetov, D.; Kolmakov, A.; McKelvey, K.; Ware, N.; El Gabaly, F.; Dunn, B.; White, H. S. Fabrication, Testing, and Simulation of All-Solid-State Three-Dimensional Li-Ion Batteries. *ACS Appl. Mater. Interfaces* **2016**, *8* (47), 32385−32391.

(13) George, S. M. Atomic Layer Deposition: An Overview. *Chem. Rev.* **2010**, *110* (1), 111−131.

(14) Meng, X.; Yang, X.-Q.; Sun, X. Emerging Applications of Atomic Layer Deposition for Lithium-Ion Battery Studies. *Adv. Mater.* **2012**, *24* (27), 3589−3615.

(15) Liu, J.; Sun, X. Elegant Design of Electrode and Electrode/electrolyte Interface in Lithium-Ion Batteries by Atomic Layer Deposition. *Nanotechnology* **2015**, *26* (2), 024001.

(16) Liu, J.; Banis, M. N.; Sun, Q.; Lushington, A.; Li, R.; et al. Rational Design of Atomic-Layer-Deposited LiFePO 4 as a High-Performance Cathode for Lithium-Ion Batteries. *Adv. Mater.* **2014**, *26* (37), 6472−6477.

(17) Li, X.; Meng, X.; Liu, J.; Geng, D.; Zhang, Y.; Banis, M. N.; Li, Y.; Yang, J.; Li, R.; Sun, X.; Cai, M.; Verbrugge, M. W. Tin Oxide with Controlled Morphology and Crystallinity by Atomic Layer Deposition onto Graphene Nanosheets for Enhanced Lithium Storage. *Adv. Funct. Mater.* **2012**, *22* (8), 1647−1654.

(18) Liu, C.; Gillette, E. I.; Chen, X.; Pearse, A. J.; Kozen, A. C.; Schroeder, M. A.; Gregorczyk, K. E.; Lee, S. B.; Rubloff, G. W. An All-in-One Nanopore Battery Array. *Nat. Nanotechnol.* **2014**, *9* (12), 1031−1039.

(19) Putkonen, M.; Aaltonen, T.; Alnes, M.; Sajavaara, T.; Nilsen, O.; Fjellvåg, H. Atomic Layer Deposition of Lithium Containing Thin Films. *J. Mater. Chem.* **2009**, *19* (46), 8767−8771.

(20) Aaltonen, T.; Alnes, M.; Nilsen, O.; Costelle, L.; Fjellvåg, H. Lanthanum Titanate and Lithium Lanthanum Titanate Thin Films Grown by Atomic Layer Deposition. *J. Mater. Chem.* **2010**, *20* (14), 2877−2881.

(21) Aaltonen, T.; Nilsen, O.; Magraso, A.; Fjellvåg, H. Atomic Layer Deposition of Li_2O-Al_2O_3 Thin Films. *Chem. Mater.* **2011**, *23*, 4669−4675.

(22) Hamalainen, J.; Holopainen, J.; Munnik, F.; Hatanpaa, T.; Heikkila, M.; Ritala, M.; Leskela, M. Lithium Phosphate Thin Films Grown by Atomic Layer Deposition. *J. Electrochem. Soc.* **2012**, *159* (3), A259−A263.
(23) Hämäläinen, J.; Munnik, F.; Hatanpää, T.; Holopainen, J.; Ritala, M.; Leskelä, M. Study of Amorphous Lithium Silicate Thin Films Grown by Atomic Layer Deposition. *J. Vac. Sci. Technol., A* **2012**, *30* (1), 01A106.
(24) Østreng, E.; Sønsteby, H. H.; Sajavaara, T.; Nilsen, O.; Fjellvåg, H. Atomic Layer Deposition of Ferroelectric $LiNbO_3$. *J. Mater. Chem. C* **2013**, *1* (27), 4283−4290.
(25) Comstock, D. J.; Elam, J. W. Mechanistic Study of Lithium Aluminum Oxide Atomic Layer Deposition. *J. Phys. Chem. C* **2013**, *117* (4), 1677−1683.
(26) Cavanagh, A. S.; Lee, Y.; Yoon, B.; George, S. M. Atomic Layer Deposition of LiOH and Li_2CO_3 Using Lithium T-Butoxide as the Lithium Source. *ECS Trans.* **2010**, *33* (2), 223−229.
(27) Østreng, E.; Vajeeston, P.; Nilsen, O.; Fjellvåg, H. Atomic Layer Deposition of Lithium Nitride and Carbonate Using Lithium Silylamide. *RSC Adv.* **2012**, *2* (15), 6315−6322.
(28) Wang, B.; Liu, J.; Sun, Q.; Xiao, B.; Li, R.; Sham, T. K.; Sun, X. Titanium Dioxide/Lithium Phosphate Nanocomposite Derived from Atomic Layer Deposition as a High-Performance Anode for Lithium Ion Batteries. *Adv. Mater. Interfaces* **2016**, *3* (21), 1600369.
(29) Miikkulainen, V.; Ruud, A.; Østreng, E.; Nilsen, O.; Laitinen, M.; Sajavaara, T.; Fjellvåg, H. Atomic Layer Deposition of Spinel Lithium Manganese Oxide via Film Body Controlled Lithium Incorporation for Thin Film Lithium Ion Batteries. *J. Phys. Chem. C* **2014**, *118*, 1258−1268.
(30) Perng, Y.-C.; Cho, J.; Membreno, D.; Cirigliano, N.; Dunn, B.; Chang, J. P. Synthesis of Ion Conducting LixAlySizO Thin Films by Atomic Layer Deposition. *J. Mater. Chem. A* **2014**, *2*, 9566−9573.
(31) Wang, B.; Liu, J.; Sun, Q.; Li, R.; Sham, T. Atomic Layer Deposition of Lithium Phosphates as Solid-State Electrolytes for All-Solid-State Microbatteries. *Nanotechnology* **2014**, *25* (50), 504007.
(32) Liu, J.; Banis, M. N.; Li, X.; Lushington, A.; Cai, M.; Li, R.; Sham, T.-K.; Sun, X. Atomic Layer Deposition of Lithium Tantalate Solid-State Electrolytes. *J. Phys. Chem. C* **2013**, *117* (39), 20260−20267.
(33) Kozen, A. C.; Pearse, A. J.; Lin, C.; Noked, M.; Rubloff, G. W. Atomic Layer Deposition of the Solid Electrolyte LiPON. *Chem. Mater.* **2015**, *27*, 5324−2331.
(34) Nisula, M.; Shindo, Y.; Koga, H.; Karppinen, M. Atomic Layer Deposition of Lithium Phosphorus Oxynitride. *Chem. Mater.* **2015**, *27*, 6987−6993.
(35) Shibata, S. Thermal Atomic Layer Deposition of Lithium Phosphorus Oxynitride as a Thin-Film Solid Electrolyte. *J. Electrochem. Soc.* **2016**, *163* (13), A2555−A2562.
(36) Pearse, A. J.; Schmitt, T. E.; Fuller, E. J.; El-Gabaly, F.; Lin, C. F.; Gerasopoulos, K.; Kozen, A. C.; Talin, A. A.; Rubloff, G.; Gregorczyk, K. E. Nanoscale Solid State Batteries Enabled by Thermal Atomic Layer Deposition of a Lithium Polyphosphazene Solid State Electrolyte. *Chem. Mater.* **2017**, *29* (8), 3740−3753.
(37) Nakagawa, A.; Kuwata, N.; Matsuda, Y.; Kawamura, J. Characterization of Stable Solid Electrolyte Lithium Silicate for Thin Film Lithium Battery. *J. Phys. Soc. Jpn.* **2010**, *79*, 98−101.
(38) Minami, T.; Hayashi, A.; Tatsumisago, M. Preparation and Characterization of Lithium Ion-Conducting Oxysulfide Glasses. *Solid State Ionics* **2000**, *136-137*, 1015−1023.
(39) Bates, J. B.; Dudney, N. J.; Gruzalski, G. R.; Zuhr, R. A.; Choudhury, A.; Luck, C. F.; Robertson, J. D. Electrical Properties of Amorphous Lithium Electrolyte Thin Films. *Solid State Ionics* **1992**, *53-56*, 647−654.
(40) Minami, T.; Hayashi, A.; Tatsumisago, M. Recent Progress of Glass and Glass-Ceramics as Solid Electrolytes for Lithium Secondary Batteries. *Solid State Ionics* **2006**, *177* (26−32), 2715−2720.
(41) Klaus, J. W.; Sneh, O.; George, S. M. Growth of SiO_2 at Room Temperature with the Use of Catalyzed Sequential Half-Reactions. *Science (Washington, DC, U. S.)* **1997**, *278* (5345), 1934−1936.
(42) Ferguson, J. D.; Smith, E. R.; Weimer, a. W.; George, S. M. ALD of SiO_2 at Room Temperature Using TEOS and H_2O with NH3 as the Catalyst. *J. Electrochem. Soc.* **2004**, *151* (8), G528−G535.
(43) Du, Y.; Du, X.; George, S. M. Mechanism of Pyridine-Catalyzed SiO 2 Atomic Layer Deposition Studied by Fourier Transform Infrared Spectroscopy. *J. Phys. Chem. C* **2007**, *111*, 219−226.
(44) Li, D.; Bancroft, G. M.; Kasrai, M.; Fleet, M. E.; Feng, X. H.; Tan, K. H.; Yang, B. X. High-Resolution Si K- and L2,3-Edge of α-Quartz and Stishovite. *Solid State Commun.* **1993**, *87* (7), 613−617.
(45) Henderson, G. S. A Si K-Edge EXAFS/XANES Study of Sodium Silicate Glasses. *J. Non-Cryst. Solids* **1995**, *183*, 43−50.
(46) Li, D.; Bancroft, G. M.; Fleet, M. E.; Feng, X. H. Silicon K-Edge XANES Spectra of Silicate Minerals. *Phys. Chem. Miner.* **1995**, *22*, 115−122.
(47) Zhang, F.; Liao, L. S.; Chan, W. H.; Lee, S. T.; Sammynaiken, R.; Sham, T. K.; Si, T. Electronic Structure of Silicon Nanowires: A Photoemission and X-Ray Absorption Study. *Phys. Rev. B: Condens. Matter Mater. Phys.* **2000**, *61* (12), 8298−8305.
(48) Henderson, G. S.; St-Amour, J. C. A Si K-Edge XANES Study of Ti Containing Alkali/alkaline-Earth Silicate Glasses. *Chem. Geol.* **2004**, *213* (1−3), 31−40.
(49) Thompson, S. P. Structural Signatures of Medium-Range Order in Annealed Laboratory Silicates. *Astron. Astrophys.* **2008**, *484* (1), 251−265.
(50) Yamada, M.; Inaba, A.; Ueda, A.; Matsumoto, K.; Iwasaki, T.; Ohzuku, T. Reaction Mechanism of "SiO"-Carbon Composite-Negative Electrode for High-Capacity Lithium-Ion Batteries. *J. Electrochem. Soc.* **2012**, *159* (10), A1630−A1635.
(51) Cabaret, D.; et al. Medium Range Structure of Borosilicate Glasses from Si K-Edge XANES: A Combined Approach Based on Multiple Scattering and Molecular Dynamics Calculations. *J. Non-Cryst. Solids* **2001**, *289* (1−3), 1−8.
(52) Cormier, L.; Gaskell, P.; Calas, G.; Soper, A. Medium-Range Order around Titanium in a Silicate Glass Studied by Neutron Diffraction with Isotopic Substitution. *Phys. Rev. B: Condens. Matter Mater. Phys.* **1998**, *58* (17), 11322−11330.
(53) Nazabal, V.; Fargin, E.; Le Flem, G.; Briois, V.; Moulin, C. C. D.; Buffeteau, T.; Desbat, B. X-Ray Absorption and Infrared Reflectance of Poled Silica Glass for Second Harmonic Generation. *J. Appl. Phys.* **2000**, *88* (11), 6245−6251.
(54) Buchner, S.; Radtke, C.; Balzaretti, N. M. Densification of Lithium Disilicate under High Pressure Investigated by XPS. *Open J. Inorg. Non-Met. Mater.* **2013**, *3* (2), 15−21.
(55) De Jong, B. H. W. S.; Ellerbroek, D.; Spek, A. L. Low-Temperature Structure of Lithium Nesosilicate, Li4SiO4, and Its Li1s and O1s X-Ray Photoelectron Spectrum. *Acta Crystallogr., Sect. B: Struct. Sci.* **1994**, *50* (5), 511−518.
(56) Soares, P. C., Jnr; Nascente, P. A. P.; Zanotto, E. D. XPS Study of Lithium Disilicate Glass Crystallisation. *Phys. Chem. Glasses* **2002**, *43* (3), 143−146.
(57) Kozen, A. C.; Pearse, A. J.; Lin, C.-F.; Schroeder, M. A.; Noked, M.; Lee, S. B.; Rubloff, G. W. Atomic Layer Deposition and in Situ Characterization of Ultraclean Lithium Oxide and Lithium Hydroxide. *J. Phys. Chem. C* **2014**, *118* (48), 27749−27753.
(58) Lu, Y.-C.; Crumlin, E. J.; Veith, G. M.; Harding, J. R.; Mutoro, E.; Baggetto, L.; Dudney, N. J.; Liu, Z.; Shao-Horn, Y. In Situ Ambient Pressure X-Ray Photoelectron Spectroscopy Studies of Lithium-Oxygen Redox Reactions. *Sci. Rep.* **2012**, *2*, 715.
(59) Yao, K. P. C.; Kwabi, D. G.; Quinlan, R. A.; Mansour, a. N.; Grimaud, A.; Lee, Y.-L.; Lu, Y.-C.; Shao-Horn, Y. Thermal Stability of Li2O2 and Li2O for Li-Air Batteries: In Situ XRD and XPS Studies. *J. Electrochem. Soc.* **2013**, *160* (6), A824−A831.
(60) Murugan, R.; Thangadurai, V.; Weppner, W. Fast Lithium Ion Conduction in Garnet-Type $Li_7La_3Zr_2O_{12}$. *Angew. Chem., Int. Ed.* **2007**, *46* (41), 7778−7781.
(61) Macdonald, J. R. Impedance Spectroscopy. *Ann. Biomed. Eng.* **1992**, *20*, 289−305.
(62) Tuller, H. L.; Button, D. P.; Uhlmann, D. R. Fast Ion Transport in Oxide Glasses. *J. Non-Cryst. Solids* **1980**, *40*, 93−118.

DOI: 10.1021/acsami.7b07113
ACS Appl. Mater. Interfaces 2017, 9, 31786−31793

(63) Prasada Rao, R.; Tho, T. D.; Adams, S. Ion Transport Pathways in Molecular Dynamics Simulated Lithium Silicate Glasses. *Solid State Ionics* **2010**, *181* (1−2), 1−6.
(64) Lammert, H.; Kunow, M.; Heuer, A. Complete Identification of Alkali Sites in Ion Conducting Lithium Silicate Glasses: A Computer Study of Ion Dynamics. *Phys. Rev. Lett.* **2003**, *90* (21), 215901.
(65) Charles, R. J. Metastable Liquid Immiscibility in Alkali Metal Oxide−Silica Systems. *J. Am. Ceram. Soc.* **1966**, *49* (2), 55−62.
(66) Neudecker, B. J.; Weppner, W. Li9SiAlO8: A Lithium Ion Electrolyte for Voltages above 5.4 V. *J. Electrochem. Soc.* **1996**, *143* (7), 2198−2203.
(67) Charles, R. J. Some Structural and Electrical Properties of Lithium Silicate Glass. *J. Am. Ceram. Soc. Soc.* **2006**, *46* (5), 460−466.
(68) Anderson, O. L.; Stuart, D. A. Calculation of Activation Energy of Ionic Conductivity in Silica Glasses by Classical Methods. *J. Am. Ceram. Soc.* **1954**, *37* (12), 573−580.
(69) Otto, K.; Milberg, M. E. Ionic Conduction in Alkali and Thallium Silicate Glasses. *J. Am. Ceram. Soc.* **1968**, *51* (6), 326−329.
(70) Dyre, J. C.; Maass, P.; Roling, B.; Sidebottom, D. L. Fundamental Questions Relating to Ion Conduction in Disordered Solids. *Rep. Prog. Phys.* **2009**, *72* (4), 046501.

DOI: 10.1021/acsami.7b07113
ACS Appl. Mater. Interfaces 2017, 9, 31786−31793